Modal amplification in active waveguides with hyperbolic dispersion at telecommunication frequencies

Joseph S. T. Smalley[1,*], Felipe Vallini[1], Boubacar Kanté[1], and Yeshaiahu Fainman[1]

[1]*University of California, San Diego, Department of Electrical and Computer Engineering, 9500 Gilman Dr., La Jolla, CA 92093, USA*

[*]*jsmalley@ucsd.edu*

Abstract: We present a method for studying amplification of electromagnetic modes in active, circularly symmetric waveguides with hyperbolic dispersion. Using this method, we obtain a closed-form expression for the modal threshold condition. We find that modal amplification is possible in a region of the radius-wavelength phase-space with small enough radius so that propagation of the mode is permitted while modal energy and phase counter-propagate. At telecommunication frequencies, such a situation is achievable only when the absolute value of the real metal permittivity exceeds that of the active dielectric. We validate our theoretical conclusions with numerical simulations that explain the threshold condition in terms of an energy balance between the longitudinal and radial components of the electric field.

OCIS codes: (160.3918) Metamaterials; (160.1190) Anisotropic optical materials; (230.7370) Waveguides; (310.6628) Subwavelength structures, nanostructures; (350.4238) Nanophotonics and photonic crystals; (250.5230) Photoluminescence.

References and Links

1. X. Zhang and Z. Liu, "Superlenses to overcome the diffraction limit," Nat. Mater. **7**(6), 435–441 (2008).
2. Z. Jacob, "The classical and quantum optics of hyperbolic metamaterials," *Thesis,* Purdue University (2010).
3. V. Veselago, "The electrodynamics of substances with simultaneously negative values of epsilon and mu," Sov. Phys. Usp. **10**(4), 509–514 (1968).
4. T. Ergin, N. Stenger, P. Brenner, J. B. Pendry, and M. Wegener, "Three-dimensional invisibility cloak at optical wavelengths," Science **328**(5976), 337–339 (2010).
5. V. Podolskiy and E. Narimanov, "Strongly anisotropic waveguide as a nonmagnetic left-handed system," Phys. Rev. B **71**(20), 201101 (2005).
6. C. Cortes, W. Newman, S. Molesky, and Z. Jacob, "Quantum nanophotonics using hyperbolic metamaterials," J. Opt. **14**(6), 063001 (2012).
7. M. Noginov, "Metamaterials with optical gain," in *Tutorials in Metamaterials*, M. Noginov and V. Podolskiy, eds. (CRC, 2012), pp. 129–161.
8. S. Xiao, V. P. Drachev, A. V. Kildishev, X. Ni, U. K. Chettiar, H. K. Yuan, and V. M. Shalaev, "Loss-free and active optical negative-index metamaterials," Nature **466**(7307), 735–738 (2010).
9. X. Ni, S. Ishii, M. D. Thoreson, V. M. Shalaev, S. Han, S. Lee, and A. V. Kildishev, "Loss-compensated and active hyperbolic metamaterials," Opt. Express **19**(25), 25242–25254 (2011).
10. R. Savelev, I. Shadrivov, P. Belov, N. Rosanov, S. Fedorov, A. Sukhorukov, and Y. Kivshar, "Loss compensation in metal-dielectric layered metamaterials," Phys. Rev. B **87**(11), 115139 (2013).
11. R. Shersby-Harvie, L. Mullett, W. Walkinshaw, J. Bell, and B. Loach, "A theoretical and experimental investigation of anisotropic-dielectric-loaded linear electron accelerators," Proc. IEE **104B,** 273–290 (1957).
12. V. M. Agranovich and V. E. Kravtsov, "Notes on crystal optics of superlattices," Solid State Commun. **55**(1), 85–90 (1985).
13. C. Chang, "Circular waveguides lined with artificial anisotropic dielectrics," IEEE Trans. Microw. Theory Tech. **20**(8), 517–523 (1972).
14. W. Yan, M. Wubs, and N. Mortensen, "Hyperbolic metamaterials: Nonlocal response regularizes broadband supersingularity," Phys. Rev. B **86**(20), 205429 (2012).
15. C. David and F. J. García de Abajo, "Spatial nonlocality in the optical response of metal nanoparticles," J. Phys. Chem. C **115**(40), 19470–19475 (2011).

#213050 - $15.00 USD Received 11 Jun 2014; accepted 11 Aug 2014; published 22 Aug 2014

16. J. Elser, V. A. Podolskiy, I. Salakhutdinov, and I. Avrutsky, "Nonlocal effects in effective-medium response of nanolayered metamaterials," Appl. Phys. Lett. **90**(19), 191109 (2007).
17. L. Coldren, S. Corzine, and M. Masanovic, "Gain and current relations," in *Diode lasers and photonic integrated circuits*, (Wiley, 2012), pp. 157–246.
18. J. Smalley, Q. Gu, and Y. Fainman, "Temperature dependence of the spontaneous emission factor in subwavelength semiconductor lasers," IEEE J. Quantum Electron. **50**(3), 175–185 (2014).
19. G. Naik, V. Shalaev, and A. Boltasseva, "Semiconductors for plasmonics and metamaterials," Phys. Status Solidi (RRL) **4**, 295–297 (2010).
20. C. Riley, T. Kieu, J. Smalley, S. Pan, S. Kim, K. Post, A. Kargar, D. Basov, X. Pan, Y. Fainman, D. Wang, and D. Sirbuly, "Plasmonic tuning of aluminum doped zinc oxide nanostructures by atomic layer deposition," *submitted to Phys. Stat. Sol. (RRL)* (2014).
21. G. V. Naik, J. Liu, A. V. Kildishev, V. M. Shalaev, and A. Boltasseva, "Demonstration of Al:ZnO as a plasmonic component for near-infrared metamaterials," Proc. Natl. Acad. Sci. U.S.A. **109**(23), 8834–8838 (2012).
22. G. V. Naik, V. M. Shalaev, and A. Boltasseva, "Alternative plasmonic materials: Beyond gold and silver," Adv. Mater. **25**(24), 3264–3294 (2013).
23. G. Naik and A. Boltasseva, "A comparitive study of semiconductor-based plasmonic metamaterials," arXiv, < http://arxiv.org/abs/1108.1531> (2011).
24. P. Johnson and R. Christy, "Optical constants of noble metals," Phys. Rev. B **6**(12), 4370–4379 (1972).
25. A. Mizrahi, V. Lomakin, B. A. Slutsky, M. P. Nezhad, L. Feng, and Y. Fainman, "Low threshold gain metal coated laser nanoresonators," Opt. Lett. **33**(11), 1261–1263 (2008).
26. J. S. Smalley, M. W. Puckett, and Y. Fainman, "Invariance of optimal composite waveguide geometries with respect to permittivity of the metal cladding," Opt. Lett. **38**(23), 5161–5164 (2013).
27. A. Govyadinov and V. Podolskiy, "Metamaterial photonic funnels for subdiffraction light compression and propagation," Phys. Rev. B **73**(15), 155108 (2006).
28. V. Podolskiy, "Anisotropic and hyperbolic metamaterials," in *Tutorials in Metamaterials*, M. Noginov and V. Podolskiy, eds. (CRC, 2012), pp. 163–207.

1. Introduction

Optical metamaterials (MMs) enable control of propagating electromagnetic (EM) energy beyond that allowed by natural materials and unachievable technologically even fifteen years ago. Possibilities enabled by MMs include focusing and imaging beyond the diffraction limit [1,2] counter propagating phase and energy, leading to opposite Cherenkov radiation and Doppler shifts [3], and last but not least, invisibility cloaking [4]. While all of these effects are tantalizing in ideal systems, realistic applications of MMs suffer from the inherent problem of dissipative losses. MMs generally also require both electrical and magnetic resonances to achieve their unique properties. While the use of hyperbolic MMs (HMMs) circumvents the requirement for magnetic resonances [5, 6], the problem of dissipative losses remains. Therefore, the theoretical understanding and experimental demonstration of lossless, or even amplified, EM wave propagation through HMMs is crucial to the continued development of nanophotonics generally and MMs in particular [7].

Amplification of propagating EM waves at ~730nm was shown experimentally in sub-wavelength thickness, dye-loaded fishnet structures, using a transient pump-probe technique [8]. Further theoretical work showed the possibility for amplification at the same wavelength of propagating EM waves in metal-dielectric layers exhibiting hyperbolic dispersion [9, 10]. These works used an organic dye under saturation as the dielectric layer to provide gain in an infinite transverse planar geometry. Improvements in sub-diffraction-limited focusing by a hyper-grating incorporating the dye were predicted to be on the order of 100% while the appearance of convective instabilities was also considered [9, 10].

In the technologically important near-infrared (NIR) telecommunication windows (1.30μm and 1.55μm), amplification of EM waves propagating through HMMs remains a problem to be solved. This is partly due to the challenge of integrating distinct materials offering metallic response and optical gain in this frequency range. Moreover, it has been unclear whether amplification is indeed possible in NIR HMMs because organic dyes, useful for amplification in the visible regime are unavailable in the NIR [7]. However, inorganic semiconductors, especially III-V compounds, which replace dyes as active media in the NIR,

#213050 - $15.00 USD Received 11 Jun 2014; accepted 11 Aug 2014; published 22 Aug 2014

offer the most practical means of achieving electrically-controlled and mass-producible HMM amplifiers.

Herein we present, to the best of our knowledge, the first theoretical proof that amplification is indeed possible in HMMs at telecommunication frequencies. We derive a closed-form expression for the region in the radius-wavelength phase-space in which modal energy is amplified in a circularly symmetric waveguide. We then confirm this derivation numerically by studying the energy balance between different components of the electric field of the propagating mode.

We first introduce the waveguide under study and recall, for self-consistency, previous work on the effective permittivity tensor for a composite material consisting of deeply subwavelength layers (Section 2). In Section 3 we investigate the requirements for active components of the effective permittivity tensor for different relative values of the real permittivities of the constituent metal and dielectric. We then investigate in Section 4 the necessary and sufficient conditions for modal amplification. In Section 5, we discuss our results, and relax several assumptions by accounting for more realistic claddings and spatial non-locality.

2. Effective anisotropy

Consider a structure composed of a periodic sequence of two distinct materials, as in Fig. 1(a). If the layer thicknesses are much smaller than the wavelength of a mode propagating in the structure, then the structure may be described equivalently as a bulk medium with anisotropic electromagnetic response [11–13]. The anisotropy is expressed by an effective permittivity tensor with elements perpendicular and parallel to the optical axis of the bulk medium, which in Fig. 1(b) corresponds to the z-direction.

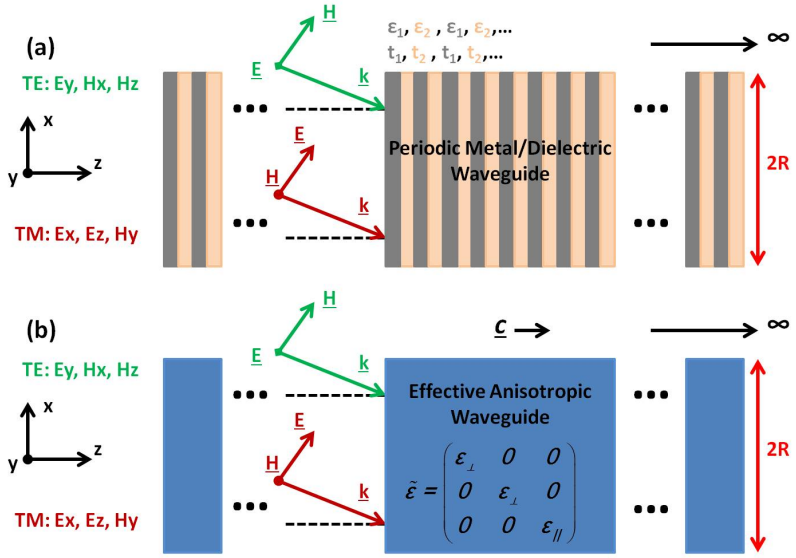

Fig. 1. Schematic of equivalent waveguides composed of (a) periodic sequence of two distinct materials and (b) bulk anisotropic effective medium. **c** denotes direction of the optical axis.

The perpendicular permittivity element arises if we consider the spatially averaged electric displacement $\langle D_{xy} \rangle$ in the x-y plane, which may be written as

$$\langle D_{xy} \rangle = \varepsilon_0 \frac{t_1 \varepsilon_1 E_{1,x} + t_2 \varepsilon_2 E_{2,x}}{t_1 + t_2} \tag{2.1}$$

#213050 - $15.00 USD Received 11 Jun 2014; accepted 11 Aug 2014; published 22 Aug 2014

where t_α, ε_α, and $E_{\alpha,x}$ are the layer thickness, relative permittivity, and tangential electric field in layer $\alpha = 1$ and $\alpha = 2$. Conservation of the tangential electric field enables us to rewrite Eq. (2.1) as

$$\left\langle D_{xy} \right\rangle = \varepsilon_\perp \varepsilon_0 E_x = \varepsilon_\perp \varepsilon_0 E_y \tag{2.2}$$

where

$$\varepsilon_\perp \equiv \frac{t_1 \varepsilon_1 + t_2 \varepsilon_2}{t_1 + t_2} \tag{2.3}$$

and the spatial averaging is justified because the electric field amplitude varies slowly compared to the rate of change of the layers. Spatial averaging of the electric field in the z-direction leads to

$$\left\langle E_z \right\rangle = \varepsilon_0^{-1} \frac{\varepsilon_1^{-1} D_{1,z} + \varepsilon_2^{-1} D_{2,z}}{t_1 + t_2}, \tag{2.4}$$

and conservation of the electric displacement normal to the interfaces enables us to rewrite Eq. (2.4) as

$$\left\langle E_z \right\rangle = \left(\varepsilon_0 \varepsilon_\parallel \right)^{-1} D_z \tag{2.5}$$

where

$$\varepsilon_\parallel \equiv \frac{\left(t_1 + t_2 \right) \varepsilon_1 \varepsilon_2}{t_1 \varepsilon_2 + t_2 \varepsilon_1}. \tag{2.6}$$

Because ε_1 and ε_2 are generally complex-valued, frequency-dependent quantities, the effective permittivities may generally be expressed as

$$\varepsilon_\perp(\omega, \boldsymbol{k}) = \varepsilon_\perp'(\omega, \boldsymbol{k}) + i\varepsilon_\perp''(\omega, \boldsymbol{k}) \tag{2.7}$$

$$\varepsilon_\parallel(\omega, \boldsymbol{k}) = \varepsilon_\parallel'(\omega, \boldsymbol{k}) + i\varepsilon_\parallel''(\omega, \boldsymbol{k}) \tag{2.8}$$

where ω and $\boldsymbol{k}$ are the temporal and spatial frequencies, respectively. The temporal dispersion arises from that of the constituent materials, whereas the spatial dispersion accounts for non-local effects, such as the finite period of the structure and electron quantization in thin layers [14–16]. Accounting for these effects is important for precise quantitative prediction of amplification properties, as we discuss in Section 5, where we compare results based on local and non-local effective medium theory (EMT). In the immediately following treatment, we use Eqs. (2.3) and (2.6) directly.

3. Requirements for active effective anisotropy

Amplification of propagating or standing waves requires that one of the constituent materials have optical gain, which is described phenomenologically by the imaginary part of the permittivity. Supposing material 1 and 2 to be metal and dielectric, respectively, and using the convention of $\exp[-i(\omega t - \boldsymbol{k}z)]$ for temporal and spatial harmonic dependence, the permittivity of the dissipative layer is written as

$$\varepsilon_1(\omega) = \varepsilon_1'(\omega) + i\varepsilon_1''(\omega) \tag{3.1}$$

while that of the active layer is

$$\varepsilon_2(\omega) = \varepsilon_2'(\omega) - i\varepsilon_2''(\omega), \tag{3.2}$$

#213050 - $15.00 USD Received 11 Jun 2014; accepted 11 Aug 2014; published 22 Aug 2014

The physical origin of the negative imaginary permittivity of Eq. (3.2) rests in a population inversion of the electronic states of the dielectric. For the inorganic semiconductors considered in this paper, population inversion refers to a system in which the density of electrons in the conduction band exceeds the density of holes in the valence bands. To achieve this non-equilibrium regime, the system requires injection of external energy, either through optical or electrical means. A great advantage of inorganic semiconductors over dye molecules as a gain media is the ease with which the material may be controllably doped for the formation of heterostructures suitable for electronic injection devices. The population inversion is directly proportional to the material gain coefficient, *g*, the latter being related to the negative imaginary permittivity of Eq. (3.2) by

$$\varepsilon_2''(\omega) = \frac{c}{\omega}\frac{g(\omega)}{\sqrt{\varepsilon_2'}}. \tag{3.3}$$

The microscopic origins of material gain in inorganic semiconductors is discussed extensively in [17]. For this work we calculate Eq. (3.3) according to [18] exactly, adding the dependence of the polarization of the EM field in the transition matrix element to account for emission coupling to transverse-magnetic (TM) modes.

To examine the requirements for active effective permittivites with notational clarity, we rewrite Eqs. (3.1) and (3.2) as

$$\varepsilon_1 = A + iB \tag{3.4}$$

and

$$\varepsilon_2 = C + iD, \tag{3.5}$$

respectively, where $A<0$, $B>0$, $C>0$, and $D<0$, descriptive of a dissipative metal and active dielectric for layers 1 and 2, respectively. Substitution of Eqs. (3.4) and (3.5) into Eq. (2.3) leads to

$$\varepsilon_\perp' = \frac{1}{2}(A + C) \tag{3.6}$$

$$\varepsilon_\perp'' = \frac{1}{2}(B + D), \tag{3.7}$$

where, for clarity, we have invoked the assumption that $t_1 = t_2$. We discuss relaxation of this assumption in Section 5. Similarly, we can substitute Eqs. (3.4) and (3.5) into Eq. (2.6) to obtain, after some algebra,

$$\varepsilon_\parallel' = 2\frac{C\left(A^2 + B^2\right) + A\left(C^2 + D^2\right)}{(A + C)^2 + (B + D)^2} \tag{3.8}$$

$$\varepsilon_\parallel'' = 2\frac{D\left(A^2 + B^2\right) + B\left(C^2 + D^2\right)}{(A + C)^2 + (B + D)^2}. \tag{3.9}$$

Using Eqs. (3.6)-(3.9), we now investigate possible situations where the imaginary effective permittivities may become positive.

3.1 Case I: $|A| < C$

When $|A|<C$, representative of, for example, a transparent conducting oxide and semiconductor at telecommunication frequencies, it follows trivially from Eq. (3.6) that $\varepsilon_\perp' > 0$. From Eq. (3.7), we find that $\varepsilon_\perp'' < 0$ requires very small metal loss or very large

#213050 - $15.00 USD Received 11 Jun 2014; accepted 11 Aug 2014; published 22 Aug 2014

dielectric optical gain. Using the fact that $AD^2 << AC^2$ and $BD^2 << BC^2$ when $C >> B$, $|D|$, we can approximate Eqs. (3.8) and (3.9) as

$$\varepsilon_{\parallel}' \cong 2\frac{C\left(A^2+B^2\right)+AC^2}{A^2+C^2-2|A|C} \tag{3.10}$$

$$\varepsilon_{\parallel}'' \cong 2\frac{D\left(A^2+B^2\right)+BC^2}{A^2+C^2-2|A|C}. \tag{3.11}$$

Examination of (3.10) shows that $\varepsilon_{\parallel}' < 0$ if $AC^2 < C(A^2 + B^2)$, which is always true for $A<0$, and examination of (3.11) shows that $\varepsilon_{\parallel}'' < 0$ requires $|D|(A^2 + B^2) > BC^2$. For an epsilon-near-zero metal, this leads to the requirement that $|D|B > C^2$, which necessitates unphysical gain. Hence for $A<0$ and $|A|<C$, an active effective permittivity tensor element is only possible in the direction orthogonal to the optical axis, and requires constituent materials with extremely favorable properties.

Recent experiments have demonstrated that aluminum-doped zinc oxide (AZO) behaves as a metal in the near-infrared, with properties heavily dependent upon the aluminum concentration [19, 20]. AZO is attractive amongst several transparent conducting oxides for NIR plasmonics, due to its low loss, an order of magnitude lower than that of silver around $\lambda = 1550$nm [21].

Indium gallium arsenide phosphide (InGaAsP) is a thoroughly studied compound semiconductor with a bandgap energy dependent upon the alloy composition. By proper tuning of the constituent elements in AZO and InGaAsP, the spectral regions wherein InGaAsP may undergo population inversion and where AZO/InGaAsP form a composite exhibiting hyperbolic dispersion may overlap.

Figure 2(a) shows such a region at a practically achievable carrier density of $N = 5\text{x}10^{18}\text{cm}^{-3}$ for an effective medium with a filling fraction (fill) of 0.5, where fill = $t_1/(t_1 + t_2)$. We have calculated the frequency dependent complex permittivities of AZO and $In_{0.564}Ga_{0.436}As_{0.933}P_{0.431}$ quantum wells using data from [22], and [17, 18], respectively, all at room temperature. Hyperbolic dispersion begins at the zero crossing of $\varepsilon_{\parallel}'$, which according to Eq. (3.10) occurs when $A = 0$, i.e., when the real permittivity of AZO is zero, at $\lambda = 1.43\mu$m. The carrier density dependence of the imaginary permittivity of InGaAsP corresponds to a pump-dependent medium. III-V semiconductors are particularly attractive in this regard because they are amenable to electronic injection of carriers, unlike the dye-based active HMMs explored in the visible regime. The emission edge of the InGaAsP is clearly visible in Fig. 2(a), near 1.62μm where $\varepsilon_{\perp}''$ quickly drops in magnitude. For this carrier density, $\varepsilon_{\perp}''$ remains positive, however, necessitating higher pumping levels to achieve an active effective medium. Figure 2(b) compares the imaginary effective permittivities for densities of $N = 1\text{x}10^{17}\text{cm}^{-3}$ and $N = 1\text{x}10^{19}\text{cm}^{-3}$. The difference in absorption and emission edges results from the dependence of the bandgap energy on the carrier concentration. We observe that $\varepsilon_{\perp}''$ changes sign in the presence of large optical gain, while $\varepsilon_{\parallel}''$ barely changes. The concentration $N = 1\text{x}10^{17}\text{cm}^{-3}$ corresponds to an equilibrium level where the InGaAsP is absorptive. Increasing the carrier concentration, and thereby the optical gain, to $1\text{x}10^{19}$ and $3\text{x}10^{19}\text{cm}^{-3}$ and $5\text{x}10^{19}\text{cm}^{-3}$, we obtain $\varepsilon_{\perp}''$ minima of –0.0292, –0.0586,

–0.0609, respectively. Thus, in principle a periodic structure of AZO/InGaAsP may behave as an active media in the direction transverse to the optical axis. However, such a property requires enormously high optical gain, $|D| > 0.300 \approx 6{,}500\text{cm}^{-1}$ at $\lambda = 1.55\mu$m, that is extremely difficult to achieve in practice.

#213050 - $15.00 USD Received 11 Jun 2014; accepted 11 Aug 2014; published 22 Aug 2014

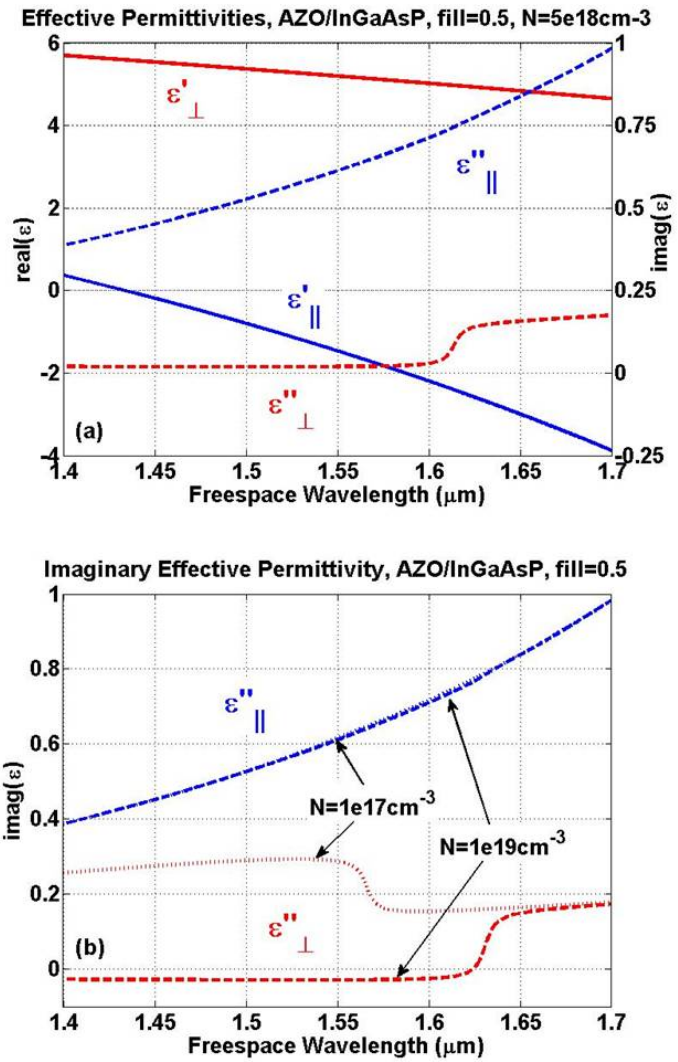

Fig. 2. (a) Real and imaginary effective permittivities, parallel and perpendicular to the optical axis of a periodic sequence of AZO and InGaAsP layers with equal thickness, for InGaAsP carrier concentration of $N = 5\text{x}10^{18}\text{cm}^{-3}$. (b) Imaginary permittivities for $N = 1\text{x}10^{17}\text{cm}^{-3}$ and $N = 1\text{x}10^{19}\text{cm}^{-3}$.

3.2 Case II: $|A| > C$

For the case where $|A|>C$, representative of, for example, a noble metal and semiconductor at telecommunication frequencies, it follows trivially from Eqs. (3.6) and (3.7) that $\varepsilon_{\perp}' < 0$ and that, for realistic metal losses and dielectric optical gain, $\varepsilon_{\perp}'' > 0$.

Based on the fact that $|A|>C$, $|A| >> B,D$, and $C >> B,D$ we can approximate Eqs. (3.8) and (3.9) as

$$\varepsilon_{\parallel}' \cong 2\frac{CA^2 + AC^2}{A^2 + C^2 - 2|A|C} \tag{3.12}$$

#213050 - $15.00 USD Received 11 Jun 2014; accepted 11 Aug 2014; published 22 Aug 2014

$$\varepsilon_{\parallel}'' \cong 2\frac{DA^2 + BC^2}{A^2 + C^2 - 2|A|C}. \tag{3.13}$$

For $|A|>C$, it follows that $\varepsilon_{\parallel}' > 0$ always, and that $\varepsilon_{\parallel}'' < 0$ requires $DA^2<BC^2$ which is always true when $D<0$. Hence, the permittivity tensor elements perpendicular and parallel to the optical axis inherit the behaviors of the constituent metal and dielectric layers, respectively, when $|A|>C$, and therefore the condition for an active effective permittivity tensor element is $|A|>C$. This conclusion is reached from a different method and offers a different interpretation of the results of [23] that long propagation lengths in surface plasmon-polariton waveguides requires noble metals, rather than transparent conducting oxides.

Noble metals exhibit losses greater than those of TCOs at telecommunication frequencies, but also have much larger real permittivities. Hence this should lead to active medium behavior in the direction parallel to the optical axis, so long as $D<0$. Figure 3 shows such behavior for a composite medium composed of silver and InGaAsP, where the complex silver permittivity is based on [24]. At carrier densities sufficient for population inversion of the InGaAsP quantum wells, we observe that the permittivity tensor parallel to the optical axis is negative. Moreover, compared to the AZO/InGaAsP example of Case I, the imaginary part of the active permittivity element is an order of magnitude larger. Hence, the approximation Eq. (3.13) is numerically verified, as is the conclusion that $\varepsilon_{\parallel}'' < 0$.

#213050 - $15.00 USD Received 11 Jun 2014; accepted 11 Aug 2014; published 22 Aug 2014

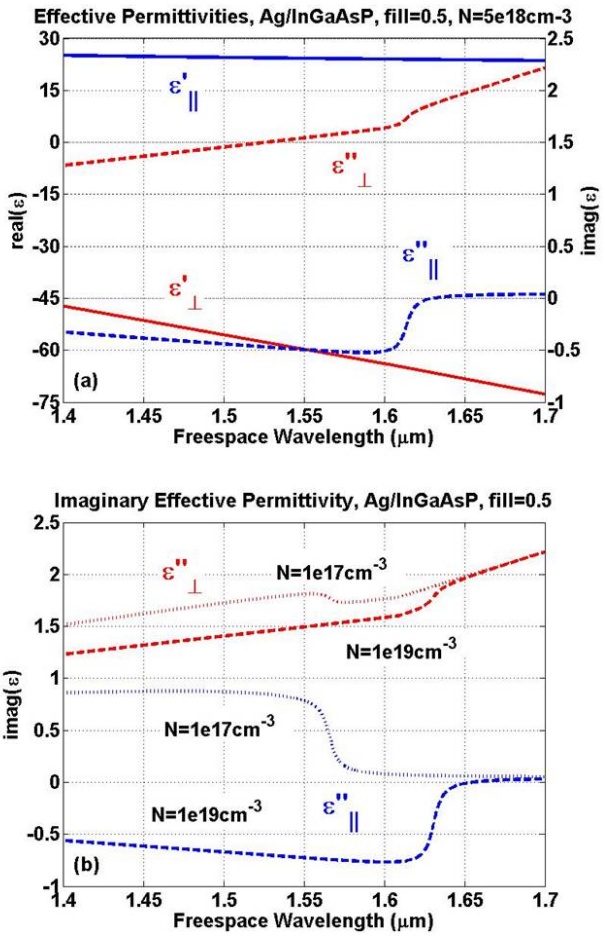

Fig. 3. (a) Real and imaginary effective permittivities, parallel and perpendicular to the optical axis of a periodic sequence of silver and InGaAsP layers with equal thickness, for InGaAsP carrier concentrations $N = 5\text{x}10^{18}\text{cm}^{-3}$. (b) Imaginary permittivities with $N = 1\text{x}10^{17}\text{cm}^{-3}$ and $N = 1\text{x}10^{19}\text{cm}^{-3}$.

3.3 Case III: $|A| \approx C$

When the magnitude of A and C are nearly equal, $\varepsilon_{\perp}'$ approaches zero, and $\varepsilon_{\perp}'' < 0$ if and only if $|D|>B$. Again this requires extremely small metal loss or large dielectric optical gain. For the permittivity element parallel to the optical axis, the condition of $|A|\sim C$ leads to the approximations of

$$\varepsilon_{\parallel}' \cong 2\frac{CA^2 - |A|C^2}{2A^2 - 2|A|C} \tag{3.14}$$

$$\varepsilon_{\parallel}'' \cong 2\frac{A^2(B+D)}{2A^2 - 2|A|C}, \tag{3.15}$$

which diverge as the magnitudes of A and C approach each other. Combining the results for $\varepsilon_{\perp}$ and $\varepsilon_{\parallel}$ suggests that this case represents a resonant condition where $\varepsilon_{\perp}$ and $\varepsilon_{\parallel}$ take the role of the dispersive and absorptive permittivites in an isotropic medium. If $|D|>B$, then

#213050 - $15.00 USD Received 11 Jun 2014; accepted 11 Aug 2014; published 22 Aug 2014

$\varepsilon_{\parallel} << 0$ and the possibility for modal amplification could be enhanced, compared to Case II, though over a narrow bandwidth.

This condition is the most difficult to achieve practically at telecommunication frequencies because the constituent materials are not readily available. For example all semiconductors that can provide optical gain in the NIR have *C* on the order of 10.

4. Requirements for modal amplification

In the previous section we have established that the presence of optical gain in a periodic sequence of metal and dielectric layers with deeply subwavelength thickness enables active response parallel to the optical axis so long as $D<0$, and may enable active response perpendicular to the optical axis for very large $|D|$. While an active medium is a necessary condition for modal amplification, it is not sufficient. The energy added to the electric field component in the direction of the active permittivity must be sufficient to offset the energy lost in the direction of the dissipative permittivity. Therefore the relative strength of the field components must be considered.

For propagation in the z-direction of Fig. 1, the modal loss is characterized by the imaginary part of the modal effective index, where, generally, the effective index is

$$\begin{aligned} n_{eff}^{(pq)}(\omega) &= n_{eff}^{\prime(pq)}(\omega) + i n_{eff}^{\prime\prime(pq)}(\omega) \\ &= \frac{1}{k_0}\left(k_z^{\prime(pq)}(\omega) + i k_z^{\prime\prime(pq)}(\omega)\right), \end{aligned} \tag{4.1}$$

with $k_0 = \omega/c$, and the superscript *pq* designating the mode number. Amplification requires that the imaginary part of one of the permittivity tensor elements is sufficiently large such that $n_{eff}^{\prime\prime}$ becomes negative. The threshold condition occurs when $n_{eff}^{\prime\prime} = 0$. We use the term threshold because an infinite waveguide serves as a zero order approximation to a laser resonator with perfectly reflecting end mirrors [25, 26]. Thus based on the active media presented in Section 4, we investigate the possibility for achieving threshold in the waveguide of Fig. 1.

We consider a circularly symmetric anisotropic waveguide with active effective permittivity in at least one direction. From [27, 28] we can determine the effective index as a function of the waveguide radius, *R*, for the aforementioned cases. To derive a closed-form expression for the cutoff and threshold radii of mode *pq*, we first consider the case of a perfect electrical conductor (PEC) cladding. Replacement of the PEC cladding by a realistic metal is discussed in Section 5. The effective index, Eq. (4.1), depends upon material and geometric parameters and is numerically found via the relation [28]

$$n_{eff}^{(pq)} = \pm\sqrt{\varepsilon_{\perp}\left(1 - \frac{\kappa_{(pq)}^2}{\varepsilon_{\parallel} k_0^2}\right)} \tag{4.2}$$

where $\kappa_{(pq)} = Z_{(pq)}/R$, with $Z_{(pq)}$ being the q^{th} zero of the p^{th} order Bessel function of the first kind. Selection of the sign of Eq. (4.2) results from the necessity that a propagating mode must satisfy $n_{eff}^{(pq)}\varepsilon_{\perp} > 0$ [28]. In the spirit of Section 3, we make use of the following notation for the complex effective index in what follows,

$$n_{eff}^{(pq)} = \pm\sqrt{(E+iF)\left[1 - \frac{\kappa_{(pq)}^2}{(G+iH)k_0^2}\right]}, \tag{4.3}$$

where

#213050 - $15.00 USD Received 11 Jun 2014; accepted 11 Aug 2014; published 22 Aug 2014

$$E \equiv \varepsilon_{\perp}', \; F \equiv \varepsilon_{\perp}'', \; G \equiv \varepsilon_{\parallel}', \; H \equiv \varepsilon_{\parallel}''. \tag{4.4}$$

4.1 Case I: $|A| < C$

The results of Section 3 showed that $\varepsilon_{\perp} > 0$ and $\varepsilon_{\parallel} < 0$ near λ_0 = 1.55μm when $|A|<C$. Therefore, positive roots of Eq. (4.3) must be selected. Case I may be summarized, using Eq. (4.4) as

$$\text{Case I}: \begin{matrix} |A| < C \\ D < 0 \end{matrix} \rightarrow \begin{matrix} E > 0, F < 0 \\ G < 0, H > 0 \end{matrix} \tag{4.5}$$

From Section 3 and (4.3) the real index may be written as

$$n_{eff}'^{(pq)} = +\sqrt{\frac{k_0^2 E\left(G^2 + H^2\right) + \kappa_{(pq)}^2 \left(E|G| + |F|H\right)}{k_0^2\left(G^2 + H^2\right)}}, \tag{4.6}$$

which clearly grows with decreasing waveguide radius and has neither lower or upper cutoff radii. The imaginary index is

$$n_{eff}''^{(pq)} = +\sqrt{\frac{\kappa_{(pq)}^2 EH - |F|\left[\kappa_{(pq)}^2 |G| + k_0^2\left(G^2 + H^2\right)\right]}{k_0^2\left(G^2 + H^2\right)}} \tag{4.7}$$

which also grows with decreasing radius if $EH>|F||G|$. Generally $H>|F|$ and $E\sim|G|$ such that $n_{eff}''^{(pq)} \propto R_{(pq)}^{-1}$ for Case I. For $R_{(pq)} < \lambda_0$, $n_{eff}''^{(pq)} \propto R_{(pq)}^{-\phi}$ with $\phi > 1$ since $\kappa_{(pq)}^2 EH > k_0^2\left(G^2 + H^2\right)$.

Figure 4(a) shows the waveguide dispersion and attenuation of the TM_{01} mode at λ = 1.55μm, for InGaAsP carrier densities of $1x10^{19}cm^{-3}$ and $5x10^{19}cm^{-3}$. The change of the real effective index with increasing optical gain is imperceptible, while the change of the imaginary index is extremely small. The weak variation with optical gain results from the fact that the TM01 mode has a strong z-component to its electric field. While $\varepsilon_{\perp}'' < 0$ for $|A|<C$, $\varepsilon_{\parallel}''$ remains positive and is several orders of magnitude larger than $|\varepsilon_{\perp}''|$. Consequently the attenuation to the z-component of the field dominates the propagation behavior. Figure 4(b) shows the logarithm of the propagation length, L, defined as $L^{(pq)} = \left(2n_{eff}''^{(pq)} k_0\right)^{-1}$, for the same mode, as a function of both waveguide radius and freespace wavelength for $N = 1x10^{19}cm^{-3}$. The increase in L at the emission edge of InGaAsP is apparent for $R>0.5$μm, however L remains finite in the R-λ phase-space, indicating that the mode is never amplified.

#213050 - $15.00 USD Received 11 Jun 2014; accepted 11 Aug 2014; published 22 Aug 2014

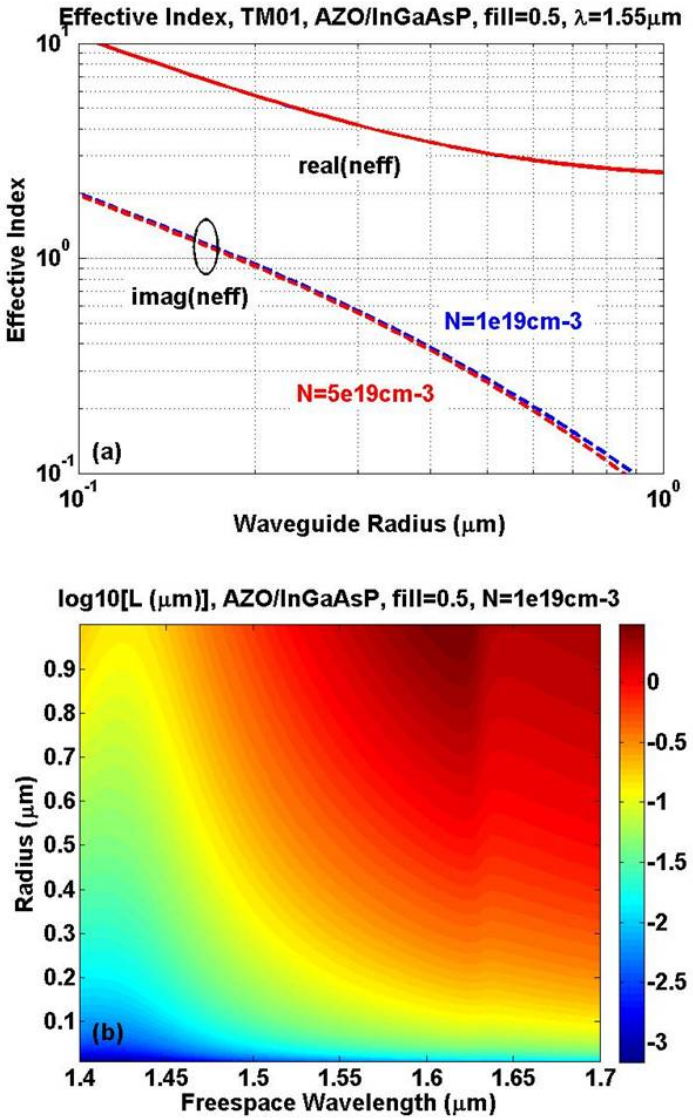

Fig. 4. (a) Effective indices of TM01 mode at λ_0 = 1.55μm as a function of the radius of AZO/InGaAsP composite waveguide with PEC cladding. (b) Contour map of log of propagation length of TM01 mode as a function of guide radius and wavelength for same structure.

4.2 Case II: $|A| > C$

When $|A|>C$, we have $\varepsilon_{\perp} < 0$ and $\varepsilon_{\parallel} > 0$ near λ_0 = 1.55μm; thus the negative root of Eq. (4.2) is selected. A consequence of this selection rule is that the waveguide has an upper limit to the cutoff radius, rather than the lower cutoff associated with conventional waveguides [28]. Using the relations that follow from Section 2, namely,

$$\text{Case II}: \begin{matrix} |A| > C \\ D < 0 \end{matrix} \rightarrow \begin{matrix} E < 0, F > 0 \\ G > 0, H < 0 \end{matrix}, \tag{4.8}$$

and inserting them into Eq. (4.2), we have for the real index

#213050 - $15.00 USD Received 11 Jun 2014; accepted 11 Aug 2014; published 22 Aug 2014

$$n_{eff}^{\prime(pq)} = -\sqrt{\frac{\kappa_{(pq)}^2\left(|E|G+F|H|\right)-k_0^2|E|\left(G^2+H^2\right)}{k_0^2\left(G^2+H^2\right)}}. \tag{4.9}$$

Setting the two terms in the numerator of Eq. (4.9) equal to each other, we may solve for the cutoff radius $R_{cut}^{(pq)}$, the radius at which the *pq* mode no longer propagates. It is

$$R_{cut}^{(pq)} = \frac{Z_{pq}}{k_0}\sqrt{\frac{|E|G+F|H|}{|E|G^2+|E|H^2}}, \tag{4.10}$$

which, may be approximated to a high degree by

$$R_{cut}^{(pq)} \simeq \frac{Z_{pq}\lambda_0}{2\pi\sqrt{G}} = \frac{Z_{pq}\lambda_0}{2\pi\sqrt{\varepsilon_{\|}^{\prime}}} \tag{4.11}$$

since $|E|G>>F|H|$ and $G^2>>H^2$. Equation (4.11) shows that for Case II structures the cutoff radius increases with the wavelength and that higher order modes have larger cutoff radii than lower order modes.

Inserting Eq. (4.8) into Eq. (4.2), we have for the imaginary index

$$n_{eff}^{\prime\prime(pq)} = -\sqrt{\frac{F\left(G^2+H^2\right)k_0^2-\left(FG-|E||H|\right)\kappa_{(pq)}^2}{k_0^2\left(G^2+H^2\right)}}. \tag{4.12}$$

Equating the two terms of the numerator, we may solve for the radius at which the mode changes from attenuating to amplifying, known as the threshold radius, $R_{thres}^{(pq)}$. It is

$$R_{thres}^{(pq)} = \frac{Z_{(pq)}}{k_0}\sqrt{\frac{FG-|E||H|}{F\left(G^2+H^2\right)}}, \tag{4.13}$$

which may be approximated by

$$R_{thres}^{(pq)} \simeq \frac{Z_{(pq)}}{k_0}\sqrt{\frac{FG-|E||H|}{FG^2}}, \tag{4.14}$$

since $G^2>>H^2$.

Combining Eqs. (4.11) and (4.14) we therefore have the necessary and sufficient conditions for modal amplification in a deeply subwavelength waveguide composed of a periodic sequence of lossy metal and active dielectric with a PEC cladding,

$$R_{thres}^{(pq)} < R^{(pq)} < R_{cut}^{(pq)}. \tag{4.15}$$

For moderate and realistic InGaAsP carrier densities [17], a region of the radius-wavelength (R-λ_0) phase-space exists satisfying Eq. (4.15). This is shown in Fig. 5(a) and 5(b), for an Ag/InGaAsP waveguide with fill = 0.5 at N = 5x10^{18}cm^{-3} and for several N values, respectively. The minimum threshold radius occurs near the emission edge of InGaAsP, and decreases towards zero with increasing optical gain. The zero-radius threshold corresponds to $|E||H|>FG$ at which point Eq. (4.14) becomes purely imaginary. The phase-space regions to the red of the emission edge of InGaAsP are a result of using the absolute value of H in (4.12)and should not be considered for amplification. Based on this result, it is clear that amplification at telecommunication frequencies requires the negative root of Eq. (4.2). Physically, this corresponds to counter propagating directions of the phase and energy.

#213050 - $15.00 USD Received 11 Jun 2014; accepted 11 Aug 2014; published 22 Aug 2014

The behavior of higher order modes is similar to that of TM01. Per Eqs. (4.11) and (4.14), the cutoff and threshold radii increase with mode order. The absolute area of the amplification phase-space also increases with mode order, as seen in Fig. 5(c), where the TM02 and TM03 are plotted alongside TM01 of Fig. 5(a). Note that the overlap of the threshold phase-space of the higher order modes with the TM01 is quite small, indicating the possibility for single-mode, low noise, amplification.

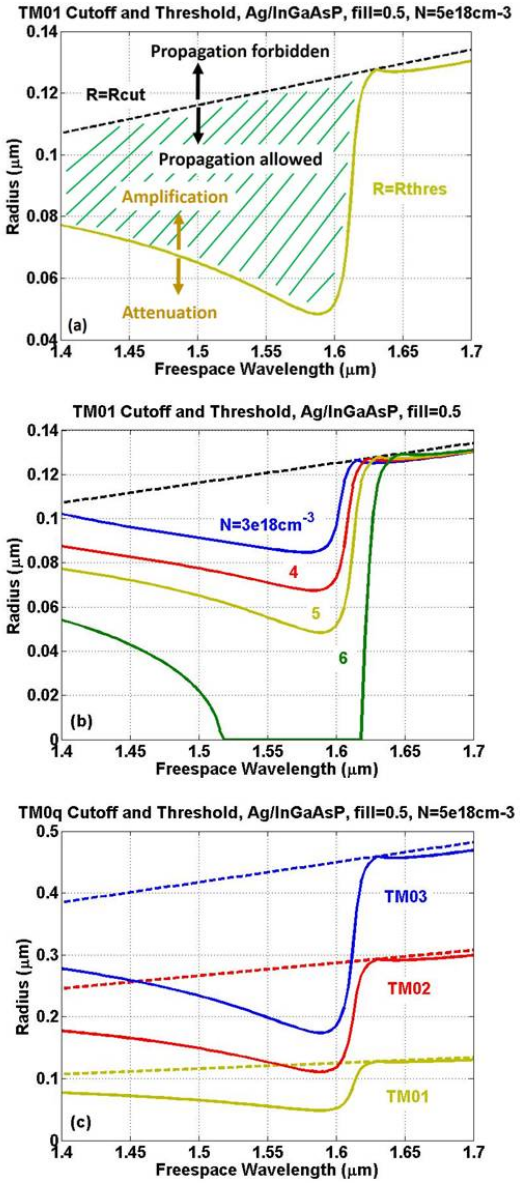

Fig. 5. Threshold and cutoff radius of TM01 mode as a function of wavelength in Ag/InGaAsP waveguide with fill = 0.5 and PEC waveguide, with (a) carrier density of 5e18cm-3, and (b) carrier density as a parameter. In (a) the hatched area corresponds to the region of phase-space satisfying Eq. (4.15). (c) Cutoff and threshold radii for TM01, TM02, and TM03 modes.

#213050 - $15.00 USD Received 11 Jun 2014; accepted 11 Aug 2014; published 22 Aug 2014

5. Discussion

Relaxation of the simplifying assumption that $t_1 = t_2$ adds an additional degree of freedom to threshold gain considerations. Intuitively, reducing the fill factor of the periodic structure would reduce the dissipative contribution of the metal to the permittivity tensor and, for $D<0$, reduce the threshold radius compared to fill = 0.5. Reduction of the metal content, however, also increases, for Case I and II, respectively, $\partial\varepsilon_{\parallel}'/\partial\lambda$ and $\partial\varepsilon_{\perp}'/\partial\lambda$ around their zero crossing. This has the consequence of red-shifting the peak of complimentary permittivities. For Case II above, the most promising for achieving amplification, the active permittivity for arbitrary filling fractions is

$$\varepsilon_{\parallel}'' = (t_1 + t_2)\frac{t_2 DA^2 + t_1 BC^2}{\left(t_2 A^2 + t_1 C^2\right)} \tag{5.1}$$

with $D<0$ and $|A|>C$. With increasing t_2/t_1 it is evident that $\varepsilon_{\parallel}''$ becomes more negative. Conversely, with decreasing t_2/t_1, $\varepsilon_{\parallel}''$ becomes less negative eventually becoming positive and eliminating the possibility for amplification.

The reason for modal amplification may be understood to follow from the balance of the modal electrical energy of the waveguide at a given cross section. Since the permeability of the constituent materials is purely real, we can ignore the magnetic energy. The electrical energy over the waveguide cross section is

$$\begin{aligned} U &= \int_{\Omega}\left(\boldsymbol{D}\cdot\boldsymbol{E}\right)dA \\ &= \int_{\Omega}\left(\varepsilon_{\perp}\left|E_{\rho}\right|^2 + \varepsilon_{\parallel}\left|E_z\right|^2\right)dA \end{aligned} \tag{5.2}$$

where E_ρ is the radial electric field component and integration is over the surface area Ω in the x-y plane of Fig. 1. The imaginary parts of the permittivites of Eq. (5.2) describe energy gained or lost. For $|A|>C$, a waveguide that amplifies mode pq must therefore satisfy

$$\frac{U_{\parallel}}{U_{\perp}} = \frac{\int_{\Omega}\left|\varepsilon_{\parallel}''\right|\left|E_z^{(pq)}\right|^2 dA}{\int_{\Omega}\left|\varepsilon_{\perp}''\right|\left|E_{\rho}^{(pq)}\right|^2 dA} > 1 \tag{5.3}$$

where $U_{\parallel}, U_{\perp}$ is the energy gained along and lost orthogonal to the optical axis, respectively. The reason for amplification of the TM01 mode can then be expressed through the dependence of the longitudinal and radial electrical field components, respectively, on the effective index, as the radius changes. These components may be written as [28]

$$E_z^{(01)} = J_0\left(Z_{(01)}\rho/R\right)\exp\left[-ik_z^{(01)}z\right] \tag{5.4}$$

$$E_{\rho}^{(01)} = ik_z^{(01)}\frac{\varepsilon_{\parallel}}{\varepsilon_{\perp}}\frac{\partial E_z^{(01)}}{\partial\rho}. \tag{5.5}$$

Without loss of generality, we can set $z = 0$ in Eq. (5.4). The integral of Eq. (5.4) is constant for different values of R due to the nature of J_0, while the integral of Eq. (5.5) decreases with radius because the radial gradient of Eq. (5.4) becomes less severe as the radius grows. Figure 6 confirms this analysis, where the value of Eq. (5.3), calculated using a commercial finite-element (FEM) solver is plotted as a function of R for several freespace telecommunication wavelengths. Perfect balance between energy lost and gained is seen to occur at $R\approx0.061\mu m$, $0.055\mu m$, and $0.048\mu m$ for $\lambda_0 = 1.50\mu m$, $1.55\mu m$, and $1.60\mu m$, respectively, in agreement with the analytically determined phase-space boundary of Fig. 5(a). We note that temporal

#213050 - $15.00 USD Received 11 Jun 2014; accepted 11 Aug 2014; published 22 Aug 2014

dispersion of the permittivities is not necessary to include in Eqs. (5.2) and (5.3) because we evaluate the expression (5.3) at individual temporal frequencies.

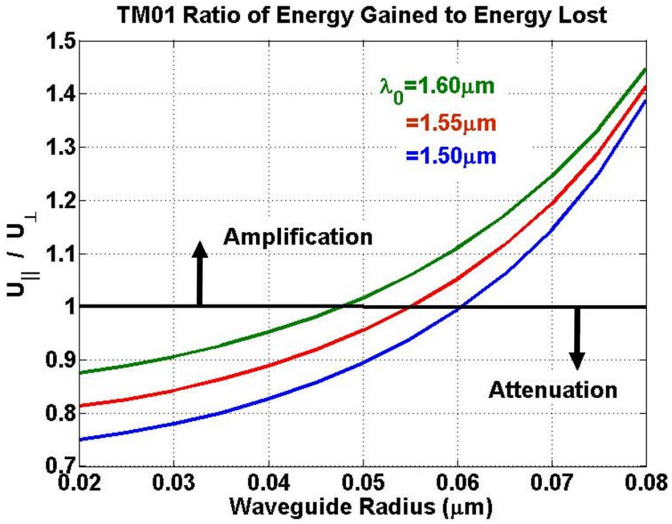

Fig. 6. Evaluation of left-hand side of Eq. (5.3) for TM01 mode at several freespace wavelengths in Ag/InGaAsP waveguide with PEC cladding. Fill = 0.5 and $N = 5\text{x}10^{18}\text{cm}^{-3}$.

Relaxation of the PEC cladding assumption results in additional losses, either due to radiation or dissipation for a real metal cladding. Real metal claddings minimize radiation loss compared to dielectric claddings at the expense of increased dissipation. For non-PEC claddings, the closed form expressions for the cutoff and threshold radii, Eqs. (4.11) and (4.14), no longer hold because the radial wavenumber $\kappa_{(pq)}$ is no longer simply proportional to the zeros of the Bessel function of the first kind.

In Fig. 7, we compare the effective index of the TM01 mode for Ag/InGaAsP waveguides with PEC and Ag claddings, calculated with FEM. The Ag cladding leads to a smaller cutoff radius, compared to the PEC cladding. However, the threshold radius decreases compared to the PEC, leading to an almost negligible change in the range of radii supporting amplification of the TM01 mode. This rather non-intuitive behavior may be understood to arise from the fact that the negative index waveguide is the antithesis of a dielectric waveguide. While the threshold radii of dielectric guides increases with more loss channels, the threshold radius of the Ag/InGaAsP waveguide decreases with increased losses. For waveguides clad with metals of finite conductivity, Eq. (5.3) becomes

$$\frac{U_{\parallel}}{U_{\perp}+U_{\text{clad}}}=\frac{\int_{\Omega}\left|\varepsilon_{\parallel}''\right|\left|E_{z}^{(pq)}\right|^{2}dA}{\int_{\Omega}\left|\varepsilon_{\perp}''\right|\left|E_{\rho}^{(pq)}\right|^{2}dA+\int_{\infty}\left|\varepsilon_{\text{clad}}''\right|\left|\boldsymbol{E}^{(pq)}\right|^{2}dA}>1, \tag{5.6}$$

where the additional term in the denominator accounts for energy dissipated in the cladding, and $\boldsymbol{E} = \boldsymbol{z}E_z + \boldsymbol{\rho}E_\rho$. For a fixed radius, the value of Eq. (5.6) may exceed that of Eq. (5.3) only because the ratio of longitudinal to radial field components of the former exceeds that of the latter. This is made possible because E_z in the non-PEC waveguide increases with decreasing radius, and at a different rate than E_ρ.

#213050 - $15.00 USD Received 11 Jun 2014; accepted 11 Aug 2014; published 22 Aug 2014

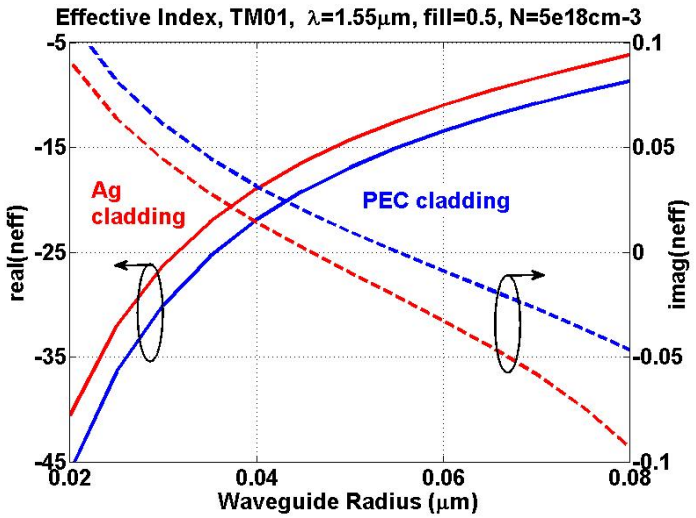

Fig. 7. Real and imaginary effective index of TM01 mode at 1.55um in Ag/InGaAsP waveguide with PEC and Ag claddings. Fill = 0.5 and $N = 5\text{x}10^{18}\text{cm}^{-3}$.

Relaxation of the local-EMT assumption by including the non-local correction to the effective permittivities [16] results in an amplification phase-space dependent upon the constituent layer thicknesses. As the layer thickness increases, the local-EMT approximation worsens, as indicated by Fig. 8, where non-locally corrected threshold radii are plotted alongside the local-EMT threshold of Fig. 5(a). The results resemble the comparison between the fundamental and higher order modes of Fig. 5(c), and clearly show that amplification phase-spaces with comparable areas exist when non-locality is taken into account.

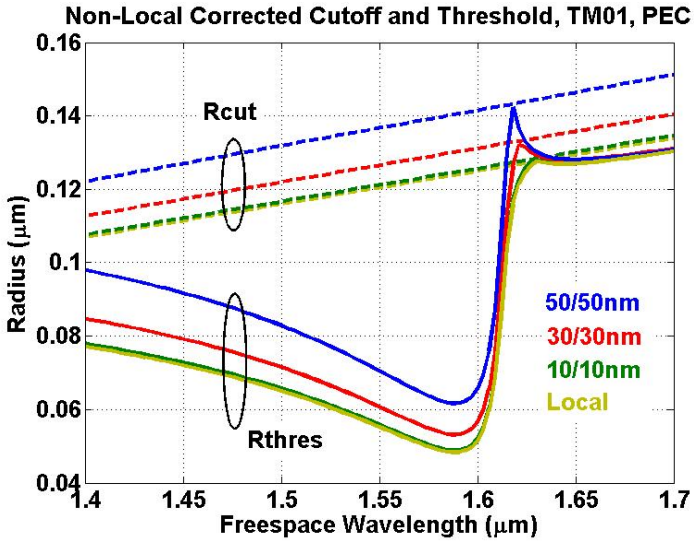

Fig. 8. Local and layer-thickness-dependent non-local correction to cutoff and threshold radii of TM01 mode at 1.55um in Ag/InGaAsP waveguide with PEC claddings. Fill = 0.5 and $N = 5\text{x}10^{18}\text{cm}^{-3}$.

6. Conclusion

We have shown theoretically that amplification of waveguide modes exhibiting hyperbolic dispersion is feasible at telecommunication frequencies. For practically achievable optical

#213050 - $15.00 USD Received 11 Jun 2014; accepted 11 Aug 2014; published 22 Aug 2014

gain levels, amplification requires that the constituent metal have a larger absolute real permittivity relative to the constituent dielectric. Furthermore, the waveguide radius must be sufficiently small such that the negative index mode propagates, while being sufficiently large such that the radial component electric field does not overwhelm the longitudinal component. While arriving at our results for waveguides with PEC cladding in the local-EMT approximation, we have shown that our theoretical results apply equally well when accounting for real claddings and spatial non-locality.

Initial experiments could include proof-of-concept amplification of modes exhibiting hyperbolic dispersion in waveguides consisting of noble metals and III-V semiconductors. More advanced work includes increasing resolution of hyperlenses and fidelity of optical cloaks using optical gain based on these proof-of-concept experiments. Additionally, this work demonstrates that active waveguides may support guided modes at telecommunication frequencies to arbitrarily small transverse dimensions, limited only by fabrication technologies.

Acknowledgments

This work was supported by the Office of Naval Research Multi-University Research Initiative (N00014-13-1-0678), the National Science Foundation (NSF) (ECE3972 & ECCS-1229677), the NSF Center for Integrated Access Networks (EEC-0812072, Sub: Y502629), the Defense Advanced Research Projects Agency (N66001-12-1-4205), and the Cymer Corporation.

#213050 - $15.00 USD Received 11 Jun 2014; accepted 11 Aug 2014; published 22 Aug 2014